Lorentz TEM Imaging of Stripe Structures Embedded in a Soft Magnetic Matrix

M. A. Basith* and S. McVitie
School of Physics and Astronomy, University of Glasgow, Glasgow G12 8QQ, United Kingdom

T. Strache, M. Fritzsche, A. Muecklich, J. Fassbender, and J. McCord†
Institute of Ion Beam Physics and Materials Research, Helmholtz-Zentrum Dresden—Rossendorf, 01314 Dresden, Germany

(Received 18 June 2015; revised manuscript received 28 August 2015; published 29 September 2015)

Néel walls in soft magnetic NiFe/NiFeGa hybrid stripe structures surrounded by a NiFe film are investigated by high-resolution Lorentz transmission-electron-microscopic imaging. An antiparallel orientation of magnetization in 1000-nm-wide neighboring unirradiated-irradiated stripes is observed by forming high-angle domain walls during magnetization reversal. Upon downscaling the stripe structure size from 1000 to 200 nm, a transition from a discrete domain pattern to an effective magnetic medium is observed for external magnetic-field reversal. This transition is associated with the vanishing ability of hosting high-angle domain walls between adjacent stripes.

DOI: 10.1103/PhysRevApplied.4.034012

I. INTRODUCTION

Magnetic patterning on a micro- and nanometer scale is of intense research interest for potential applications in sensors [1] and bit-patterned media for high-density data-storage applications [2]. By lateral magnetic patterning of ferromagnetic thin films using ion irradiation, the magnetic properties such as saturation magnetization [3–7] and anisotropy [8–10] can be changed on a local scale. If the patterning size is chosen below certain intrinsic magnetic length scales, the patterned medium may show properties not observed in either the original film or in an equivalent film with changed magnetic properties. Ion irradiation has been used to pattern periodic ferromagnetic (FM) stripe array structures where FM stripes of different saturation magnetization are present [5,11]. Such periodic stripelike pattern of the ion-beam-modified films [11,12] has proven already the strong influence of the length scale of the lateral patterning [13] on the micromagnetic behavior of the hybrid material [5,6]. Compared to conventional techniques like reactive ion etching, ion-beam-assisted patterning provides additional advantages like the possibility to locally modify magnetic properties [13–15] without multistep deposition processes using different materials [11].

In this paper, we look at irradiated FM stripes which have lateral dimensions on the micron and submicron length scale. This is significant, as one of the fundamental length scales which can be used to initially explore the modified magnetic structures is that of the domain-wall width. The width associated with the tails of a Néel wall extends over several micrometers in soft magnetic $Ni_{81}Fe_{19}$ thin films [16]. The Néel wall width does not depend only on the material properties but also on the geometry and the lateral dimensions [17] of the microstructure where it is located. Here we report on magnetic hybrid structures consisting of arrays of periodic stripes which are produced by magnetic patterning, where the patterning is realized by local irradiation of the film by Ga^+ focused-ion-beam (FIB) irradiation [10]. The aim of the magnetic patterning is to produce localized regions with reduced magnetization. In previous investigations, the domain configurations were studied in periodic stripe structures for stripe width equal to and above the micron length scale [5,6,11]. During external field reversal along the stripe axis, densely packed nearly 180° interstripe domain walls are created for stripe widths of these dimensions. These interstripe domain walls mediate exchange spring behavior on a lateral basis [5]. While this behavior is of considerable interest, it prompts further investigations, in particular, the nature of the domain configurations at the interface of the modulated periodic stripe structures on a length scale well below the exchange-correlation length (typically 10–1000 nm).

In order to image periodic stripe structures under the micron length scale and to exploit the scaling limits of this kind of structure, high-resolution Lorentz transmission-electron-microscopy (TEM) imaging [18] and, in particular, the differential-phase-contrast (DPC) mode of Lorentz microscopy is well suited for such structures [19]. The DPC method is particularly well suited for this study, as it provides direct visualization of domains and domain walls as well as quantitative induction maps on the nanometer length scale [20,21]. The DPC technique is invaluable where the induction strength (and sample thickness) varies

*Department of Physics, Bangladesh University of Engineering and Technology, Dhaka-1000, Bangladesh.
mabasith@phy.buet.ac.bd
†Institute for Materials Science, University of Kiel, 24143 Kiel, Germany.

as it does in exchange spring systems. Examples of small lateral magnetic structures imaged by high-spatial-resolution Lorentz TEM imaging include observation of the spin configuration across ferromagnetic domains in $La_{0.325}Pr_{0.3}Ca_{0.375}MnO_3$ films [22] and measurement of magnetocrystalline anisotropy and domain-wall widths in $La_{0.67}Sr_{0.33}MnO_3$ films [23].

Therefore, in this investigation, the influence of the downscaling of the patterning size on the domain-wall formation and the magnetization-reversal processes in saturation-magnetization-modulated stripe structures are studied by structural and quantitative Lorentz TEM imaging. Furthermore, an explanation of the magnetic behavior of the stripe patterns is investigated using micromagnetic modeling.

II. EXPERIMENTAL DETAILS

For the experiments, polycrystalline $Ni_{81}Fe_{19}$ (atomic percent) films of nominal 20 nm thickness are deposited by magnetron sputtering on top of Si_3N_4 window membranes [24] suitable for TEM investigations. During the deposition of the magnetic material, an external magnetic field is applied to produce a magnetization-induced magnetic anisotropy. Magnetic hybrid structures consisting of arrays of periodic stripes structures, as shown in Fig. 1, are produced by magnetic patterning. The aim of the magnetic patterning is the local reduction of the saturation magnetization of the material. The long axis of the stripes is aligned parallel to the anisotropy axis of the $Ni_{81}Fe_{19}$ film. The patterning is realized by Ga^+ focused-ion-beam-irradiation-based lithography. A typical pattern is shown in a scanning-electron-microscope (SEM) image in Fig. 1(a) where the film exhibits irradiated rectangular areas of dimensions of $1 \times 20\ \mu m^2$. The focused-ion-beam-irradiation parameters are energy of 30-keV Ga^+, current of 10 pA, ion dose of $1000\,\mu C/cm^2$ (6.24×10^{15} ions/cm^2), step size of 6 nm, dwell time of 0.036 ms resulting in a beam speed of 0.167 mm/s. Each stripe is irradiated once without any repetition.

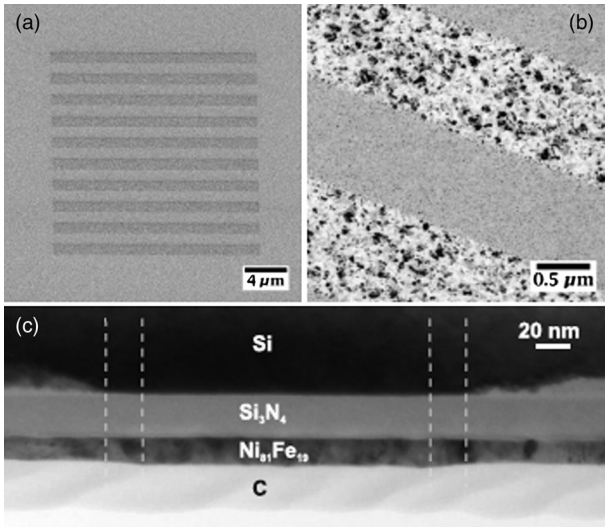

FIG. 1. Scanning-electron-microscopy image (a) of FIB written stripe array and plan-view bright-field TEM image (b). The stripe width in both cases is 1 μm. Cross-sectional TEM image (c) of an unirradiated area between two FIB irradiated stripes whose edges are indicated by the white dashed lines (stripe width 200 nm).

III. RESULTS AND DISCUSSION

A. Structural and magnetic characterization

As an illustration of the changes in both film morphology and magnetic properties due to local ion irradiation, we present here an exemplary detailed study for the case of FIB irradiation. The plan-view bright-field (BF) TEM image in Fig. 1(b) shows both irradiated and unirradiated stripes with a width of 1000 nm. The unirradiated and irradiated regions can easily be distinguished, as the irradiation causes considerable increase in the grain size from 5–10 nm to 30–40 nm. An increase of grain size after Ga^+ focused-ion-beam irradiation of NiFe films has also been reported earlier [25–28]. A cross-sectional TEM BF image of a stripe pattern of 200-nm stripe width located on a frame of a silicon-nitride membrane is shown in Fig. 1(c). The irradiated layer stack can be recognized by the reduced thickness due to irradiation-induced sputtering [Fig. 1(c)]. The actual thickness deposited and of the irradiated $Ni_{81}Fe_{19}$ layer is determined to be 16.9 ± 0.5 nm and 14 ± 0.5 nm, respectively. TRIDYN [29] simulations of the irradiation process of the layer system $Ni_{81}Fe_{19}$ (16.9 nm)/Si_3N_4 (25 nm)/Si suggest an inhomogeneous gallium profile with a maximum concentration of 5.1% at a penetration depth of 8.7 nm and a surface recession of 2 nm. The value of the surface recession is in reasonable agreement with the measured changes in film thickness. The magnetization configuration during external field reversal inside the stripe patterns is imaged by means of Lorentz microscopy [20,30] in the Fresnel and differential-phase-contrast (DPC) mode. The DPC mode is practiced on a scanning-transmission-electron microscope. Initially, low-angle electron-diffraction [20,31] experiments are carried out in the TEM to measure the difference of the product of saturation induction B_S and film thickness t, $B_S t$, between the unirradiated and irradiated areas of the film. Using the Fresnel mode of Lorentz TEM, a 180° domain wall is formed along the stripe pattern during reversal so that oppositely magnetized domains in both regions are present, as shown in Fig. 2(a), where the wall is visible as a black line. Fine scale structure due to magnetization ripple can been seen; this runs perpendicularly to the direction of magnetization allowing arrows to be assigned to either side of the wall. Therefore, pairs of diffraction spots are formed by illuminating the area (marked by the red circle) of the antiparallel alignment of magnetization [Fig. 2(a)]. In Fig. 2(b), four diffraction

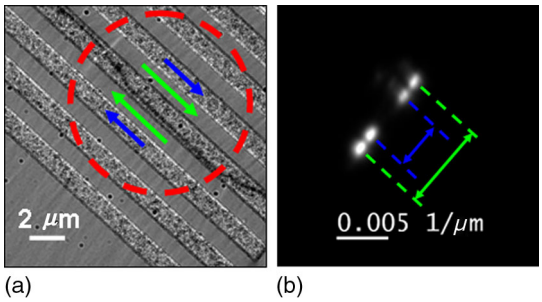

FIG. 2. (a) Fresnel image showing the oppositely magnetized magnetic region of the unirradiated and irradiated stripes. Green and blue arrows denote magnetization in the unirradiated and irradiated stripes, respectively. A 180° domain wall (black line in image) is clearly visible along the stripe pattern between the regions of opposite magnetization. (b) Electron-diffracted spots are obtained by illuminating the area marked by the red circle in image (a) from low-angle-diffraction experiments using Lorentz TEM. The two outer spots (indicated by the green marking) arise from the unirradiated regions, whereas two inner spots (indicated by blue) are from the irradiated regions.

spots are observed for the stripe pattern—two from oppositely magnetized unirradiated regions (green marked) and the other two from the oppositely magnetized regions with reduced saturation-magnetization value and film thickness (blue marked). The ratio of the values of $B_S t$ (and, hence, the magnetic moment) between the irradiated and unirradiated stripes is 60%. For a decrease in film thickness of 2.9 nm as obtained from cross-sectional TEM measurements, the magnetic induction B_S is calculated to be 72% of the value in the unirradiated stripe, i.e., as deposited film. In the next stage of this investigation, the magnetization-reversal processes in saturation-magnetization-modulated stripe structures of widths 1000 and 200 nm are presented.

B. Reversal processes in stripe width 1000 nm

The magnetization reversal inside the modulated film is first studied for a stripe width of 1000 nm by Fresnel imaging and is shown in Fig. 3. The sample is initially saturated along the long axis of the stripe with a negative external field which is then reduced to zero. Subsequently, the field is then increased in the positive direction. In Fig. 3, with the field at 1 Oe, it can be seen that the continuous film region reverses while the magnetization in the patterned region remains in the negative direction. This is apparent as domain walls are clearly visible at either side of the long edges of the patterned region. From the magnetization ripple visible (not apparent at displayed size) inside the as-prepared soft magnetic $Ni_{81}Fe_{19}$ film, the magnetization orientation is deduced (large red arrows). The magnetization direction inside the irradiated material (small red arrows) cannot be deduced directly, as no sufficient magnetization ripple contrast is present there. Therefore, the magnetization direction is calculated based on

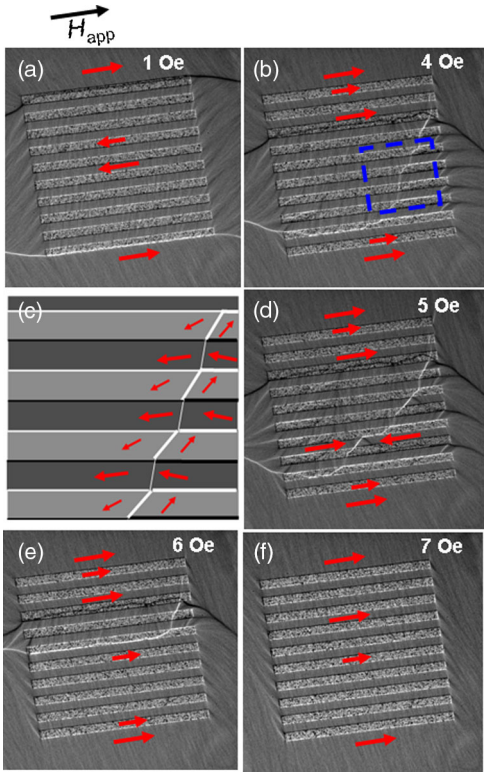

FIG. 3. Fresnel image sequence [(a),(b),(d)–(f)] of the magnetization reversal inside the magnetization-modulated film. (c) A schematic of blue marked region of Fresnel image (b). The irradiated stripes are shown in lighter gray. The nominal stripe width is 1000 nm.

magnetic-flux density-continuation arguments, assuming a continuous magnetic induction perpendicular across the stripes. Because of different film thickness and different saturation-magnetization values, an alternating dark and bright Fresnel contrast is apparent at the interfaces between the unirradiated and irradiated stripes [this is very clearly visible in Fig. 2(a)]. The domain walls separating the continuous film and the stripe pattern have much higher contrast than the lines between the unirradiated and irradiated regions, as the walls have a 180° change in magnetization direction, whereas between the stripe region, the magnetization changes between different strengths of parallel magnetization.

On increasing the strength of the applied field to 4 Oe [Fig. 3(b)], the irradiated stripes start to reverse their magnetization. Spikelike domains nucleate at the stripe's ends, and the related walls propagate along the stripes. Similar to extended hybrid stripe patterns [5], a collective reversal of magnetization of the irradiated stripes is observed, as shown in the blue-square-marked region of Fig. 3(b) and its schematic Fig. 3(c). These domain walls separate areas of nearly opposite magnetization orientations inside the irradiated stripes, being high-angle walls. However, associated walls are also present in the non-irradiated stripes. There, they separate areas with

magnetization orientations slightly tilted in respect to each other, being low-angle walls. Therefore, areas of neighboring stripes are seen to exist with opposite longitudinal magnetization components separated by high-angle domain walls at the stripe interfaces [Fig. 3(b)]. This is also indicated in the schematic Fig. 3(c) where the stripe interfaces are shown to have strong bright and dark contrast in this region, consistent with the contrast in the image in Fig. 3(b). Furthermore, in Fig. 3(b), the high-angle domain walls first seen in Fig. 3(a) extending into the surrounding film and formerly located at the outer irradiated stripes are observed to have moved already to the inside of the stripe pattern. Because of this movement, the magnetization reverses completely in all the stripes traversed by these walls. It should be noted that these walls are only ever seen in the irradiated stripes and not in the unirradiated stripes. Obviously, it is energetically more favorable to locate these walls in the irradiated material due to smaller values of both saturation magnetization and film thickness. Upon further increase of the external field value, the magnetization inside the unirradiated stripes starts reversing before the irradiated stripes complete their reversal [Fig. 3(d)]. Domain walls propagating along the unirradiated stripes are pinned, and transverse domain walls are formed only inside the unirradiated stripes [Fig. 3(d)]. The transverse walls are similar in form to walls observed in patterned nanowires [28]. The reversal of the hybrid structure is influenced by the high-angle domain walls in the surrounding film which are initially pinned at the outer structure regions. These domain walls move when the external field exceeds the appropriate depinning fields [Fig. 3(e)] and the hybrid structure finally completes the magnetization reversal [Fig. 3(f)].

Looking at the reversal process of the stripes, it can be determined whether the unirradiated or irradiated stripes with high or low saturation-magnetization value, respectively, start the magnetization reversal. The increased coercivity in the irradiated stripes with low saturation-magnetization value support a switching of the unirradiated stripes with high saturation-magnetization value. Notably, changes of the magnetization reversal along the initial easy axis are measured for $70 \times 70\ \mu m^2$ squares of a $Ni_{81}Fe_{19}\,(20\ nm)/Si_3N_4$ reference sample irradiated with a focused ion beam with the same parameters. The coercivity H_c increases to at least 6 Oe due to an increase in pinning of the domain walls. However, by considering the difference in energy between the two regions, it will be expected that the energy associated with the irradiated region is lower due to lower moment and possibly exchange. Therefore, a switching of these irradiated stripes first is expected. Obviously, this seems to be the dominant part, and the fact that the DWs reside in the irradiated stripe is an indication of this. To support this argument, micromagnetic simulations are carried out and results will be presented in Sec. III D.

Details of the magnetization orientations of the formerly described magnetization pattern of Fig. 3(b) are now discussed. The magnetization-reversal cycle is repeated in order to produce a similar domain geometry, as shown in Fresnel image Fig. 4(a). By switching from Fresnel to DPC imaging and then imaging the area indicated in Fig. 4(a), the magnetic-induction components parallel [Fig. 4(b)] and perpendicular [Fig. 4(c)] to the stripe axis are mapped. In the lower right edge of the panel in Fig. 4(a) (blue rectangle), again a reversal in a part of the irradiated material can be observed to have started. The mapped magnetic-induction component perpendicular to the stripe axis [Fig. 4(c)] shows a transverse-magnetization component in both irradiated and unirradiated stripes. Despite this transverse-magnetization component, periodic antiparallel magnetization components

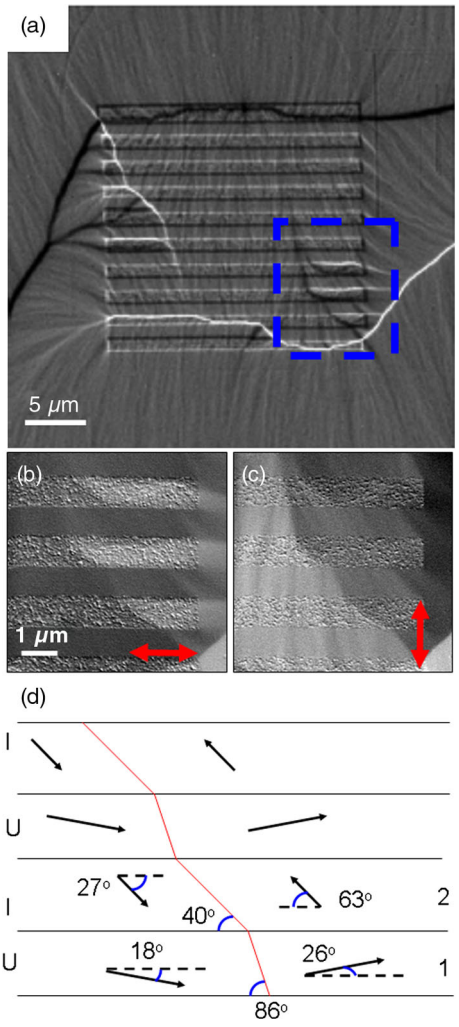

FIG. 4. High-resolution differential phase-contrast imaging of a magnetization state during field reversal. The two sensitivities are shown by double-headed arrows. The stripe width is 1 μm. The wall contrast of the Fresnel image (a) can be directly compared with both magnetic-induction components [(b),(c)] mapped by DPC imaging. Induction components in (b),(c) are shown schematically in (d).

along the stripe axis are present [Fig. 4(b)]. Magnetization components in Figs. 4(b) and 4(c) are shown schematically in Fig. 4(d) along with the rotation angles measured from these DPC images. The calculation is based on consistency between the signal levels on the two components, the wall angles, and the assumption of no net charge on the walls and interfaces. Such assumptions are consistent with the normal component of magnetic induction being continuous (i.e., $\nabla \cdot \mathbf{B} = 0$) [32] across a boundary, whereas the transverse component may be discontinuous. It should be noted that the contrast normal to the boundaries between the irradiated and unirradiated regions in Fig. 4(c) shows a continuity of this component of induction in that the contrast levels are observed not to change across the boundary. The transverse components can be seen to change [Fig. 4(b)] as expected. The angles of the walls and induction at the interfaces are calculated based on the DPC image contrast level together with the saturation-magnetic-induction values measured from low-angle-diffraction data given in Sec. III A.

As shown in the Fresnel image [Fig. 3(d)] where the reversal starts in the irradiated stripes, what happens in the application of a reverse field is that there is a rotation of the magnetization in the stripes. At low fields, this rotation is fairly small in the unirradiated stripes. If there is to be no charge at the interface, then there is a much larger rotation in the irradiated stripes and we get a larger angle DW there. This larger/smaller rotation in the irradiated/unirradiated stripe is, in fact, what we see from the schematic shown in Fig. 4(d). If we consider the unirradiated and irradiated stripes 1 and 2, respectively, in the schematic Fig. 4(d), it is clear that this state is consistent with no net charge being present at the interfaces and walls. Therefore, a larger rotation of magnetization in the irradiated stripe is expected by forming high-angle DWs.

In our experiments, we are not able to observe a complete antiparallel magnetization alignment in neighboring stripes. In such a case, the tails of two neighboring Néel walls (located at the interfaces of the stripes) must fit into the dimension of one stripe's width. Obviously, the dimension of the tails is much larger, so the high-angle domain walls between neighboring stripes are densely packed, but the overlapping tails of the Néel walls do not allow for a complete antiparallel alignment.

C. Reversal processes in stripe width 200 nm

The effect of increasing the interaction of the densely packed high-angle domain walls between the stripes on the magnetization reversal of the hybrid structure is studied by scaling the patterning size down to a stripe width of 200 nm. In Fig. 5, differential phase contrast images for a representative domain state during external magnetic-field reversal of a 200-nm wire width are shown. The mapped magnetic-induction component is parallel or longitudinal (perpendicular or transverse) to the stripes are shown by double-headed arrows.

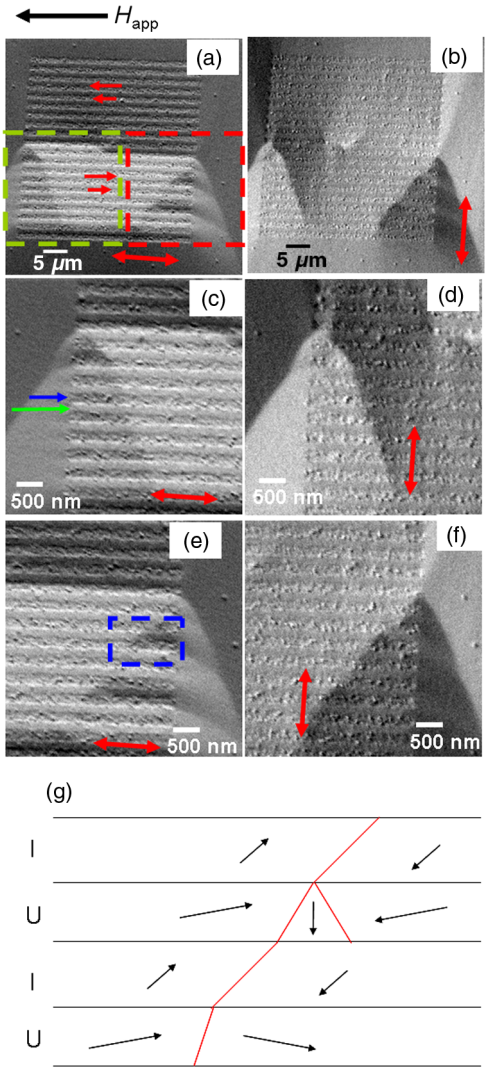

FIG. 5. DPC images of stripe array with stripe width of 200 nm. The two sensitivities are shown by double-headed arrows. Images (a),(b) show the magnetic-induction distribution for the whole hybrid structure. Images (c),(d) [(e),(f)] show the magnification of the green and red rectangular regions, respectively, of image (a). The two arrows in image (c) denote the unirradiated (green) and irradiated (blue) stripes. (g) The schematic of the marked region in DPC image (e).

The pair of images Figs. 5(a) and 5(b) shows the magnetic-induction distribution for the whole hybrid structure. The upper-situated stripes as indicated by the red arrows [Fig. 5(a)] can be seen to have already completed reversal, and these stripes are magnetized along the external field direction. In the pair of images Figs. 5(c) and 5(d), a magnified region of the left lower part (green rectangle) of the structure is shown. Here, comparing the longitudinal and transverse-magnetization component, it is evident that the low-angle wall separates areas with slightly different magnetization orientations. Not only is the magnetization inside the stripes with low saturation-magnetization value rotating away from the stripe axis, but also the

magnetization in the stripes with high value follow this rotation for the reason of flux continuity. Also, from the angle of the low-angle wall with respect to the stripe axis, it can be deduced that the magnetization at the stripes' ends has a transverse component. Apparently, no discrete pattern with antiparallel alignments of the magnetization of the neighboring stripes is found, which is observed for wider stripes in Figs. 3 and 4. In the pair of images Figs. 5(e) and 5(f), a magnification into the right lower part (red rectangle) of the structure is shown. Compared to the left structure side, the domain wall is a high-angle wall for two irradiated stripes inside the blue rectangular region of Fig. 5(e). The magnetization of this blue rectangle region is shown in the schematic diagram, Fig. 5(g). Inside the two irradiated stripes, the magnetization has opposite longitudinal components on both sides of the wall. Therefore, high-angle domain walls are formed at the interfaces of the reversed irradiated stripe and the neighboring unirradiated stripe. In the unirradiated stripes, we see that both a head-to-head wall (upper stripe) is supported and a low-angle wall (lower stripe) can be supported, but periodic neighboring high-angle domain walls between adjacent stripes, which are observed for wider stripes (1000 nm), are not found in these narrower stripes. Instead of this, the stripes tend to reverse together. Therefore, the patterning size provides an effective magnetic medium, as was reported for a 2-μm-width stripe pattern embedded in a weakly antiferromagnetically exchange-coupled $Co_{90}Fe_{10}/Ru/Co_{90}Fe_{10}$ trilayer system [11]. Notably, in Ref. [11], the magnetic-reversal behavior of micrometer-size stripe patterns achieved by ion irradiation in a weakly antiferromagnetically exchange-coupled $Co_{90}Fe_{10}/Ru/Co_{90}Fe_{10}$ system is explained by modification of magnetic-material properties, e.g., anisotropy and saturation magnetization. Although the stripe width was much larger, i.e., 2 μm compared to that of 200 nm fabricated in our system, however, that observation indicates interactions of the internal magnetization of embedded stripes with the adjacent ones in the unirradiated antiferromagnetically coupled trilayers. In our investigation, the formation of densely packed high-angle Néel walls between the narrower stripes is, therefore, suppressed for this structure size.

D. Micromagnetic simulation on stripe patterns

The two-step reversal of the irradiated stripes of width 1000 nm is attributed to the lower energy of the domain walls in this region. To support this argument, micromagnetic simulations using the OOMMF package [33] are carried out for an assembly of two neighboring stripes with different values of saturation magnetization M_S and exchange stiffness constant A. The dimensions of each stripe and the cell size of the simulation are chosen to be 4 μm $\times$ 200 nm $\times$ 20 nm and $5 \times 5 \times 5$ nm^3, respectively. Inside the simulation, the magnetic-material parameters are used as follows: saturation magnetization $M_{S,1} = 8.6 \times 10^6$ A/m, exchange stiffness constant $A_{11} = 1.3 \times 10^{11}$ J/m, and anisotropy constant $K = 0$. A damping coefficient α of 0.5, though not typical for $Ni_{81}Fe_{19}$ is used in order to speed up the relaxation of the micromagnetic configurations. The saturation-magnetization value of the neighboring stripe with reduced values is $M_{S,2}$ at 60% compared to the initial value of $M_{S,1}$. The exchange stiffness constant A_{22} of the stripe with reduced saturation-magnetization value and the exchange-coupling stiffness constant between the stripes A_{12} are estimated with the relations (1) and (2) [34].

$$A_{22} = A_{11}\left(\frac{M_{s,\text{irradiated}}}{M_{s,\text{unirradiated}}}\right)^2 = 4.68 \times 10^{-12}\ \text{J/m}, \quad (1)$$

$$A_{12} = A_{21} = 0.5(A_{11} + A_{22}) = 8.84 \times 10^{-12}\ \text{J/m}. \quad (2)$$

A schematic cross section of the two neighboring stripes is illustrated in Fig. 6(a). First, an initial magnetization configuration [Fig. 6(b)] with a 180° domain wall in the stripe with saturation magnetization $M_{S,1}$ is set and relaxed at zero external field to the domain state shown in Fig. 6(c).

The initially configured 180° domain wall is not stable, and a flux closure pattern is formed on relaxation, hosting a high-angle domain wall near the interface of both stripes. This domain wall is located in the stripe with reduced saturation-magnetization value $M_{S,2}$ due to the lower wall energy and not at the interface itself. For the rest of the

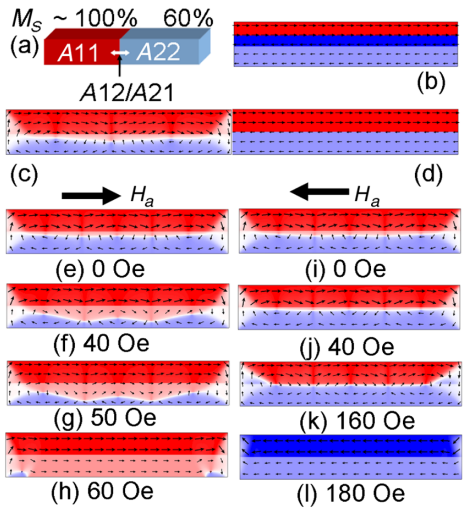

FIG. 6. Schematic cross section (a) of a stripe assembly simulated in OOMMF with different saturation-magnetization values M_S, exchange stiffness constants A_{11}, A_{22}, and coupling constant A_{12}. After initializing the magnetization states (b),(d), the magnetization relaxes into a flux closure pattern [(c), (e), and (i)]. The movement of the formed high-angle domain wall near the interface of the two stripes for two different external field directions H_a is shown in (e)–(h) and (i)–(l). The dimensions of each stripe and the cell size of the simulation are chosen to be 4 μm $\times$ 200 nm $\times$ 20 nm and $5 \times 5 \times 5$ nm^3, respectively.

simulations, an initial magnetization state with a 180° domain wall at the interface of both stripes [Fig. 6(d)] is used where the relaxed state [Figs. 6(e) and 6(i)] is almost equal to the previous state [Fig. 6(c)]. The displacement of the high-angle domain wall upon the application of a magnetic field along the stripe axis for two opposite field directions is studied; see Figs. 6(e)–6(l). It is apparent that the domain wall is free to move in the stripe (with changed magnetic parameters), reversing finally the magnetization in this stripe in the applied field direction [Figs. 6(e)–6(h)]. Applying the field antiparallel to the magnetization of the lower stripe [Figs. 6(j)–6(l)] with reduced saturation magnetization $M_{S,2}$ in the relaxed state, the domain wall gets pinned close to the interface between the stripes [Figs. 6(j) and 6(k)]. In this case, the reversal of the magnetization in the stripe with saturation-magnetization value $M_{S,1}$ is completed by rotation of the moments inside the stripe instead of moving the high-angle domain wall across the energy barrier. This different field-direction-dependent behavior confirms the impact of the reduction in wall energy due to the reduction of the saturation-magnetization value on the reversal mechanisms. This reduction in wall energy ultimately supports the argument that irradiated stripes start the reversal process during the experiments.

IV. CONCLUSIONS

Saturation-magnetization-modulated stripes embedded in a $Ni_{81}Fe_{19}$ matrix are investigated regarding the occurrence of antiparallel magnetization components for adjacent stripes. Starting from a stripe width of 1000 nm, a pronounced two-step reversal with nearly antiparallel-orientated magnetization in neighboring stripes is observed. It is evident that there is no net charge present at the interfaces and walls. Therefore, a larger rotation of magnetization in the irradiated stripe is observed by forming high-angle DWs. However, the spacing between the neighboring nearly 180° domain walls still allows for discrete stripe domain patterns. By scaling the patterning size down to a stripe width of 200 nm, we observe a transition in the characteristic magnetization patterns during external field reversal. Because of strong domain-wall tail interactions in adjacent stripes, the formation of neighboring high-angle DWs at the interfaces of these stripes is suppressed. Therefore, a tendency of collective reversal of the stripe pattern is observed. The difference in behavior between the 1000- and 200-nm-wide stripes makes the studied system an interesting starting point to further investigate the domain-wall configurations in such saturation-magnetization-modulated stripe structures. The lateral interfaces between the antiparallel-aligned directions of magnetization allow direct characterization of the lateral exchange spring magnetization via Lorentz microscopy. This is in contrast to conventional exchange spring systems, which are based on the formation of a planar interfacial domain wall [5]. We anticipate that the results obtained also have wide implications for additional magnetic systems where different magnetic phases interact laterally at an interface and can provide important insight into exploring and understanding lateral exchange spring structure behavior.

ACKNOWLEDGMENTS

The authors thank R. Mattheis and K. Kirch from IPTH Jena for film deposition. Funding by DAAD-ARC and Grant No. DFG FA 314/3-2 is acknowledged.

[1] M. Diegel, S. Glathe, R. Mattheis, M. Scherzinger, and E. Halder, A new four bit magnetic domain wall based multiturn counter, IEEE Trans. Magn. **45**, 3792 (2009).
[2] B. C. Stipe, T. C. Strand, C. C. Poon, H. Balamane, T. D. Boone, J. A. Katine, J.-L. Li, V. Rawat, H. Nemoto, A. Hirotsune, O. Hellwig, R. Ruiz, E. Dobisz, D. S. Kercher, N. Robertson, T. R. Albrecht, and B. D. Terris, Magnetic recording at 1.5 pb m-2 using an integrated plasmonic antenna, Nat. Photonics **4**, 484 (2010).
[3] L. Folks, R. E. Fontana, B. A. Gurney, J. R. Childress, S. Maat, J. A. Katine, J. E. E. Baglin, and A. J. Kellock, Localized magnetic modification of permalloy using Cr^+ ion implantation, J. Phys. D **36**, 2601 (2003).
[4] D. McGrouther and J. N. Chapman, Nanopatterning of a thin ferromagnetic CoFe film by focused-ion-beam irradiation, Appl. Phys. Lett. **87**, 022507 (2005).
[5] J. McCord, L. Schultz, and J. Fassbender, Hybrid soft-magnetic lateral exchange spring films prepared by ion irradiation, Adv. Mater. **20**, 2090 (2008).
[6] J. Fassbender, T. Strache, M. O. Liedke, D. Marko, S. Wintz, K. Lenz, A. Keller, S. Facsko, I. Mönc, and J. McCord, Introducing artificial length scales to tailor magnetic properties, New J. Phys. **11**, 125002 (2009).
[7] I. Barsukov, F. M. Römer, R. Meckenstock, K. Lenz, J. Lindner, S. Hemken to Krax, A. Banholzer, M. Körner, J. Grebing, J. Fassbender, and M. Farle, Frequency dependence of spin relaxation in periodic systems, Phys. Rev. B **84**, 140410(R) (2011).
[8] S. I. Woods, S. Ingvarsson, J. R. Kirtley, H. F. Hamann, and R. H. Koch, Local magnetic anisotropy control in NiFe thin films via ion irradiation, Appl. Phys. Lett. **81**, 1267 (2002).
[9] J. McCord, T. Gemming, L. Schultz, J. Fassbender, M. O. Liedke, M. Frommberger, and E. Quandt, Magnetic anisotropy and domain patterning of amorphous films by He-ion irradiation, Appl. Phys. Lett. **86**, 162502 (2005).
[10] J. McCord, I. Mönc, J. Fassbender, A. Gerber, and E. Quandt, Local setting of magnetic anisotropy in amorphous films by Co ion implantation, J. Phys. D **42**, 055006 (2009).
[11] M. Langer, A. Neudert, J. I. Mönch, R. Mattheis, K. Lenz, J. Fassbender, and J. McCord, Magneto-optical analysis of stripe elements embedded in a synthetic antiferromagnet, Phys. Rev. B **89**, 064411 (2014).
[12] C. Hamann, R. Mattheis, I. Mönc, J. Fassbender, L. Schultz, and J. McCord, Magnetization dynamics of magnetic

domain wall imprinted magnetic films, New J. Phys. **16**, 023010 (2014).

[13] R. Bali, S. Wintz, F. Meutzner, R. Hübner, R. Boucher, A. A. Ünal, S. Valencia, A. Neudert, K. Potzger, J. Bauch, F. Kronast, S. Facsko, J. Lindner, and J. Fassbender, Printing nearly-discrete magnetic patterns using chemical disorder induced ferromagnetism, Nano Lett. **14**, 435 (2014).

[14] M. A. Basith, S. McVitie, D. McGrouther, and J. N. Chapman, Reproducible domain wall pinning by linear non-topographic features in a ferromagnetic nanowire, Appl. Phys. Lett. **100**, 232402 (2012).

[15] M. J. Benitez, M. A. Basith, R. J. Lamb, D. McGrouther, S. McFadzean, D. A. MacLaren, A. Hrabec, C. H. Marrows, and S. McVitie, Engineering Magnetic Domain-Wall Structure in Permalloy Nanowires, Phys. Rev. Applied **3**, 034008 (2015).

[16] A. Hubert and R. Schaefer, *Magnetic Domains* (Springer, New York, 1998), Chap. 3.6.4, pp. 223–241.

[17] P.-O. Jubert, R. Allenspach, and A. Bischof, Magnetic domain walls in constrained geometries, Phys. Rev. B **69**, 220410(R) (2004).

[18] S. McVitie, D. McGrouther, S. McFadzean, D. A. MacLaren, K. J. O'Shea, and M. J. Benitez, Aberration corrected Lorentz scanning transmission electron microscopy, Ultramicroscopy **152**, 57 (2015).

[19] J. N. Chapman, I. R. McFadyen, and S. McVitie, Modified differential phase contrast Lorentz microscopy for improved imaging of magnetic structures, IEEE Trans. Magn. **26**, 1506 (1990).

[20] J. N. Chapman, The investigation of magnetic domain structures in thin foils by electron microscopy, J. Phys. D **17**, 623 (1984).

[21] M. L. De Graef, in *Proceedings of 2002 IEEE International Magnetics Conference, Amsterdam, 2002* (IEEE, New York, 2002).

[22] J. Q. He, V. V. Volkov, M. Beleggia, T. Asaka, J. Tao, M. A. Schofield, and Y. Zhu, Ferromagnetic domain structures and spin configurations measured in doped manganite, Phys. Rev. B **81**, 094427 (2010).

[23] K. J. O'Shea, D. A. MacLaren, D. McGrouther, D. Schwarzbach, M. Jungbauer, S. Hühn, V. Moshnyaga, and R. L. Stamps, Nanoscale mapping of the magnetic properties of (111)-oriented $La_{0.67}Sr_{0.33}MnO_3$, Nano Lett. **15**, 5868 (2015).

[24] M. Ruehrig, B. Khamsehpour, K. Kirk, J. Chapman, P. Aitchison, S. McVitie, and C. Wilkinson, The fabrication and magnetic properties of acicular magnetic nano-elements, IEEE Trans. Magn. **32**, 4452 (1996).

[25] C.-M. Park and J. Bain, Local degradation of magnetic properties in magnetic thin films irradiated by Ga^+ focused-ion- beams, IEEE Trans. Magn. **38**, 2237 (2002).

[26] C.-M. Park and J. A. Bain, Focused- ion-beam induced grain growth in magnetic materials for recording heads, J. Appl. Phys. **91**, 6830 (2002).

[27] D. Ozkaya L, R. M. Langford, W. L. Chan, and A. K. Petford-Long, Effect of Ga implantation on the magnetic properties of permalloy thin films, J. Appl. Phys. **91**, 9937 (2002).

[28] M. A. Basith, S. McVitie, D. McGrouther, J. N. Chapman, and J. M. R. Weaver, Direct comparison of domain wall behavior in permalloy nanowires patterned by electron beam lithography and focused ion beam milling, J. Appl. Phys. **110**, 083904 (2011).

[29] W. Moeller, W. Eckstein, and J. P. Biersack, Tridyn-binary collision simulation of atomic collisions and dynamic composition changes in solids, Comput. Phys. Commun. **51**, 355 (1988).

[30] J. N. Chapman, A. B. Johnston, L. J. Heyderman, S. McVitie, W. A. P. Nicholson, and B. Bormans, Coherent magnetic imaging by TEM, IEEE Trans. Magn. **30**, 4479 (1994).

[31] Y. Togawa, T. Koyama, K. Takayanagi, S. Mori, Y. Kousaka, J. Akimitsu, S. Nishihara, K. Inoue, A. S. Ovchinnikov, and J. Kishine, Chiral Magnetic Soliton Lattice on a Chiral Helimagnet, Phys. Rev. Lett. **108**, 107202 (2012).

[32] C. H. Marrows, Spin-polarised currents and magnetic domain walls, Adv. Phys. **54**, 585 (2005).

[33] M. J. Donahue and D. G. Porter, National Institute of Standards and Technology, Report No. nistir 6376, 1999.

[34] R. Schaefer, Domains in, 'extremely', soft magnetic materials, J. Magn. Magn. Mater. **215–216**, 652 (2000).